

The Effect of Discrete Blowing Jets on Submerged Inlet Flow Uniformity

T. Reynolds¹ and M. F. Reeder²

*Air Force Institute of Technology, WPAFB, Ohio, 45433**

An experimental flow control study was performed on a submerged inlet, with a geometry documented by NACA, to determine whether discrete blowing would offset the boundary layer deficit created at the throat and, subsequently, the engine face. Measurements of the uniformity of the streamwise velocity, secondary flow patterns, and turbulence statistics were determined non-intrusively using three-component laser Doppler velocimetry (LDV). The throat had a rectangular cross-section (7.14 cm²) and the flow was incompressible (less than Mach 0.1) for all cases. Mass flow addition rates ranging from 0.5% to 7% of the main flow through the inlet was applied. In addition to blowing rate, the effect of the location of flow control ports was examined. In two cases, blowing was introduced at the inception of the ramp so that the flow followed the surface. In the remaining two cases, the port locations were placed approximately one third of the distance closer to the throat, approximately one third, closer to the inlet. For each port location, the effect of angling, or skewing, the ports toward the corners was investigated. The experiment showed that jets positioned closer to the inlet generally yielded more uniform flow per mass addition, suggesting that the jets from the individual ports were well-mixed with the primary stream. This result matched predictions based on a simple jet mixing model.

NOMENCLATURE

u/u_{av}	=	Dimensionless Streamwise (x -direction) velocity component
v/u_{av}	=	Dimensionless Y -direction velocity component
w/u_{av}	=	Dimensionless Z -direction velocity component
u'/u_{av}	=	Dimensionless fluctuating velocity component (\bar{u}' , \bar{v}' , \bar{w}')
$u'v'/u_{av}^2$	=	Dimensionless $\overline{u'v'}$ cross component of the Reynolds stress, as are $\overline{u'w'}$, $\overline{v'w'}$,
u_i	=	Laser Doppler velocimetry measurement components
m_r	=	The mass flow ratio of the flow control to that measured for the inlet
u_{av}	=	Average measured throat velocity
u_{av}/u_∞	=	Average throat velocity compared to the tunnel free stream velocity
i	=	Variable number (1–3)

1. INTRODUCTION

Submerged inlets, which by definition are recessed into the body of the aircraft, were initially considered in the 1940's and 1950's with the hypothesis that overall efficiency might be increased relative to a scoop inlet due to a reduction in the drag profile [1]. The studies did not continue further since the pressure losses that were incurred from the boundary layer tended to offset the advantages of a decreased wetted area [2–5]. In the original studies, a NACA submerged inlet was altered and examined to determine the causes of the pressure losses and possible methods of improvement. The influence of the boundary layer and of the induced vortices formed from the flow over the ramp sidewalls were predicted by Mossman and Randall [2]. The appeal of the submerged inlet design was lessened in part because the losses led to limitations on the engine's capabilities over a large range of flight conditions. To put this early work in perspective, the submerged inlet designs were generally planned for aircraft with two submerged inlets, with one on each side of the aircraft. With some

¹ graduate student, Aerospace Engineer, Air Force Institute of Technology.

² Associate Professor, PhD, Department of Aeronautics and Astronautics.

* The views expressed in this article are those of the authors and do not reflect the official policy or position of the United States Air Force, Department of Defense, or the U.S. Government.

exceptions, it was concluded that submerged inlet designs were generally no more efficient than scoop or pod hung engines [3]. For that reason, submerged inlets are almost non-existent for civil aircraft. An excellent review of the submerged inlets as it relates to other inlet styles is given by Sobester [6].

In recent years, survivability considerations have led to a resurgence of interest in submerged inlets for military aircraft. Designers generally wish to create short engine passageways while reducing susceptibility of the aircraft by keeping any metal components of the compressor out of view. The submerged inlet can be designed to meet this criterion although more aggressive curvature can lead to boundary layer growth, separation and vortex induced losses [4,7]. Various methods have been considered, both in the original NACA studies and in much more recent investigations to deal with these losses. Most examinations could be categorized as passive geometry changes, which are geometrically fixed and continuously alter the flow [2, 8–9].

Researchers have examined aspect ratios, ramp angles and sidewall configurations, each directed towards altering the flow uniformity. The aspect ratio was found to be favorable in general towards a greater height than width, the width being in the spanwise direction and the height being the direction into the aircraft body, for an opening. The benefit was due to the comparative percentage of boundary layer ingested and vortex entering the inlet [2,7,10]. Similar reasons for the amount of boundary layer ingested, also holds true for the ramp angle. A balance of the boundary layer growth while avoiding separation was necessary, since too much growth meant a larger portion of the ingested flow was sluggish. However, if the inlet angle was too aggressive, separation occurred, leading to more incurred losses [2,10]. The wall divergence was changed to attenuate the wall vortex to even out the flow profile [11]. The vortex in some instances could be used to thin the boundary layer and improve the flow quality entering the submerged inlet [2,8]. Many of the more recent studies involved computational studies to optimize the inlet shape based upon specified parameters [9,10].

Alteration of the interior duct geometry to even out the velocity and pressure profiles is another flow control method that has been used. Some extensive studies have been reported, that have been promising at the studied conditions [10,12]. One example is the use of a fin, the fin creates a small vortex off the tip that alters the flow profile [13], and another was an indentation within the inlet surface [14]. In the study by Jovanovic et al. [13], a passive flow control method was used to bring about improved uniformity. The results from their computational study indicated that the fin was adding a secondary flow component. The swirl off the tip of fin was the controlling feature that created a more uniform inlet profile. They examined the inlet profile using the velocity computed from the computational study and compared their results to experiments conducted with a hot-film anemometer. Because the results were collected for one component of the velocity, the secondary velocity components were not validated. Taskinoglu and Knight [14] did, however, investigate changes in the secondary flow in subsequent computational studies. A passive method was used to alter the inlet uniformity in a circular duct through the use of four different indentation configurations in the inlet wall. The profile was more uniform with the application of the flow control.

Active flow control, in the form of blowing or suction, has some advantages in that it could be more easily turned on or off when needed. Using the bleed air is one possible means of enacting active flow control upon the boundary layer. It can be costly in terms of engine performance since the high pressure air cannot be used for thrust. However, if the flow uniformity can be gained with only a small percentage of mass flow addition, then the thrust penalty might become acceptable, especially if the control is only implemented for limited flight regimes. Studies have shown that active flow control methods in serpentine inlets and curved duct geometries are effective for improving uniformity and in reducing pressure losses [4-5,15-16]. This study was performed in an effort to further the use of active flow control as a potential means of improving the inlet profile.

Conceptually, an active flow control method could be affected by the same onboard computer system that controls the engine throttling and measurements. A schedule could be programmed into the computer for the flight condition to attenuate the flow at various flight regimes for the expected boundary layer and air flow. Additionally, the active flow control could be used in more aggressively curved inlet duct configurations than a passive method. The active flow control could be implemented directly at the source of the curvature to force reattachment of the flow and eliminate the separation losses, as was shown by Rabe et al. [4]. Takeoff and landing conditions are a small portion of the flight regime, however, they encounter the greatest potential for separation due to the aircraft angle of attack generating additional flow curvature into the inlet. The takeoff and landing conditions will have low flight speeds but high inlet velocities in comparison to cruise conditions.

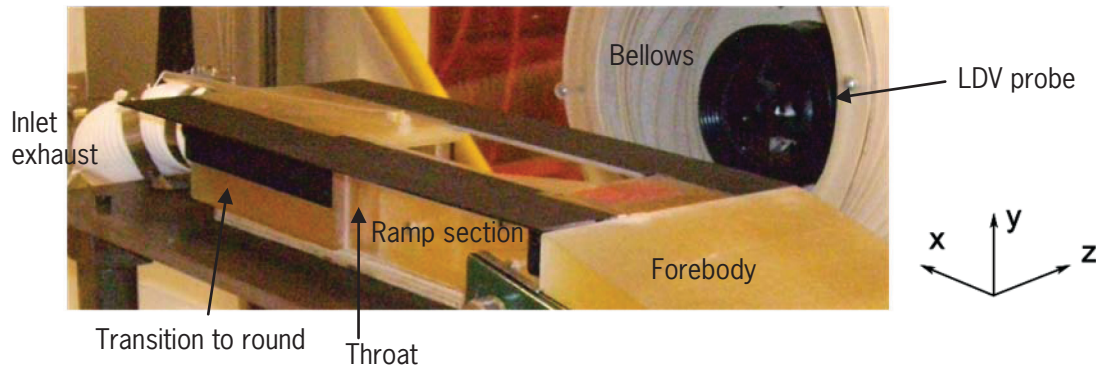


Figure 1: Submerged inlet model resting on the plate with the simulated forebody and body made of plates to inhibit forebody wake ingestion. The free stream flow is in the positive x -direction.

2. EXPERIMENTAL PROCEDURE

Much of the design and fabrication of the inlet was conducted using rapid prototyping with an EDEN 333 Objet/Polyjet Strata system, commonly described as a 3-D printer or rapid prototyper. These parts were drawn in SolidWorks®, and exported to stereolithography formatted files. The resolution of the parts, which are plastic (FullCure M-720 model material) were built using the 3-D printer. The EDEN 333 has a nominal resolution of 84 μm . The model of the submerged inlet is shown in Figure 1. It was built in three sections: the forebody, the ramp and the transition to round section. The throat of the inlet, where most measurements were carried out, was located just upstream of the transition-to-round section. Flow control was applied to the inlet via the section with the ramp, and the solid part drawings allowed for straightforward modification of the flow paths for different flow control options. A total of four different ramp sections were built and used interchangeably during the course of the experiment.

The model was mounted in the AFIT low speed wind tunnel, which is described in more detail in Reeder et al. [22], with a 0.84 m by 1.05 m cross section. For data presented here, free stream velocities were held constant at approximately 30 m/s. Measured turbulence intensity suggested levels less than one percent in the free stream for these conditions.

Each section of the plastic model was bolted to a steel backing plate and connected with fasteners to ensure the model was secure during testing. The plate and model were attached to steel posts which were secured to the wind tunnel floor. A flexible hose was connected to the exit of the model to draw air through the inlet. The diameter of the hose was approximately twice as large as the exit diameter of the model to reduce influence on the upstream flow. The hose exited the wind tunnel and was coupled to the suction port of a 5 Hp blower, nominally capable of a maximum flow rate of 0.0991 cubic meters per second. The actual mass flow through the inlet was monitored using a Rosemount Model 285 Annubar® meter with an accuracy of approximately 1 standard liter per minute (SLPM), which was mounted just downstream of the exit of the blower. A mass flow regulator (Omega FMA-2600A/FVL-2600A series) maintained a constant mass flow rate through the system without dependency on pressure variation for the flow control. The sidewalls of the ramp section of the submerged inlet were composed of clear optical grade Plexiglas to allow optical access. These clear sidewalls extended onto the transition piece to a location just downstream of the throat.

Figure 2 displays a top view of four different flow control configurations placed within the ramp section. For each, the air used for active flow control was brought into a cavity, shown with dashed lines, located within the ramp section. The piping was attached to the model and exited the tunnel to the blower to simulate the engine. The only section changed during the tests was the ramp section. The straight step configuration and the fanned step configuration had the flow control positioned at the beginning of the ramp. The straight ramp and fanned ramp had the step removed with a continuation of the ramp angle upstream so a clean ramp profile was created. The flow control holes were positioned further downstream and integrated into the ramp surface. The velocity ratios for a mass flow ratio, m_r , are given in Table 1 for all of the flow configurations examined in this study. The average throat velocity was 49 m/s.

The overall configuration can be seen in Figure 3. In the step configurations the holes were located at the beginning of the ramp, approximately 33% of the overall length from the leading edge of the ramp section. The holes for the ramp configuration were downstream of the ramp section leading edge

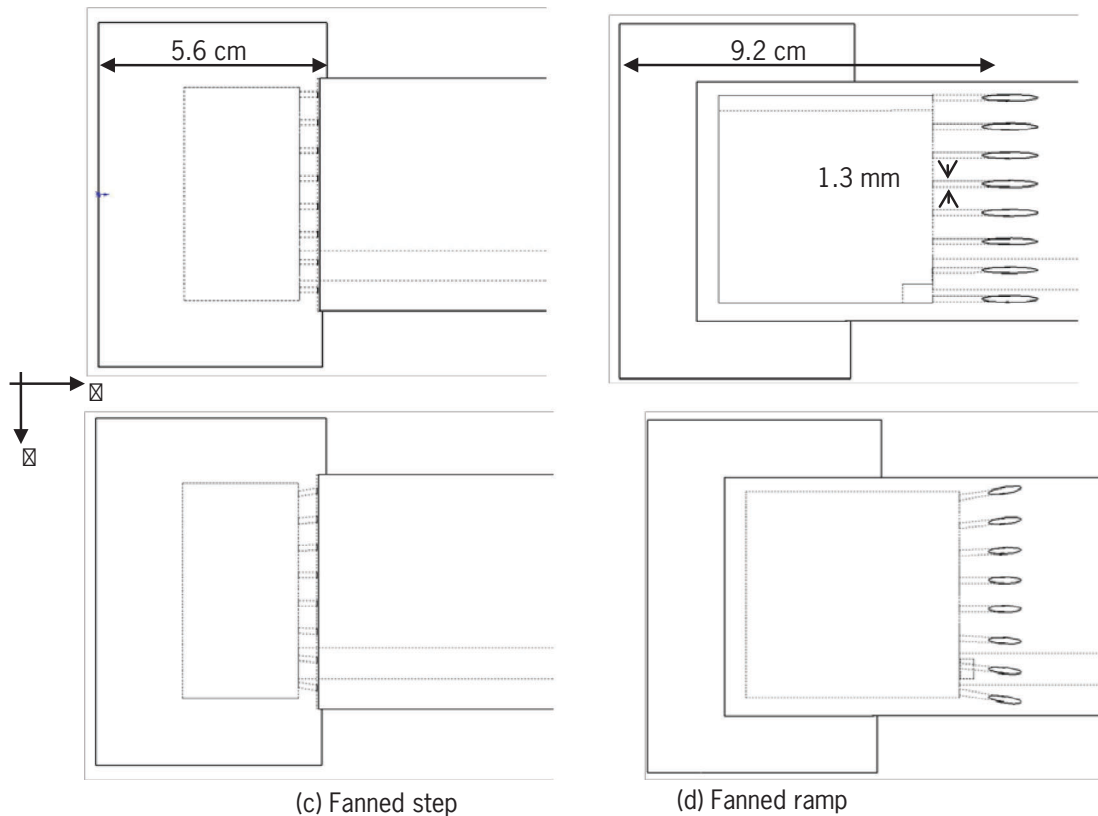


Figure 2: Flow control configurations as viewed from the top (positive y -axis). The x - and z - axes are indicated at the left of the figure.

by approximately 43%. A total of eight holes were used for the purposes of symmetry and guaranteed through jet spreading theory that the ramp surface would be covered uniformly by the time the flow reached the throat.

The fanned configurations were chosen to direct energy towards the expected wall vortex that is created by the flow over the sidewall into the ramp entrance [11]. The fanning angles of the flow control holes were zero degrees for the middle two holes with the angles increasing by three degrees as the holes progressed outward towards the walls. The holes nearest the wall were angled nine degrees relative to the flow in the spanwise (z) direction. The number of holes and their spacing were evaluated by examination of free jet growth and mixing theory. The spacing between the holes (6.8 mm) was used to estimate the distance along the ramp necessary for the profiles to become indistinguishable to within a five percent variation [17]. Free jet mixing theory predicted an ample mixing length to accomplish the task. The jet profiles became indistinguishable well before the throat in both jet locations and configurations. A large margin for error was left to ensure a sufficient mixing length was provided to prevent creating additional variations to the throat velocity profile [18].

Table 1: The jet exit velocity ratio for a given mass flow percentage, m_r

m_r	v_j/u_{av}
0	0
0.005	0.30
0.01	0.60
0.015	0.90
0.02	1.20
0.05	3.02
0.07	4.23

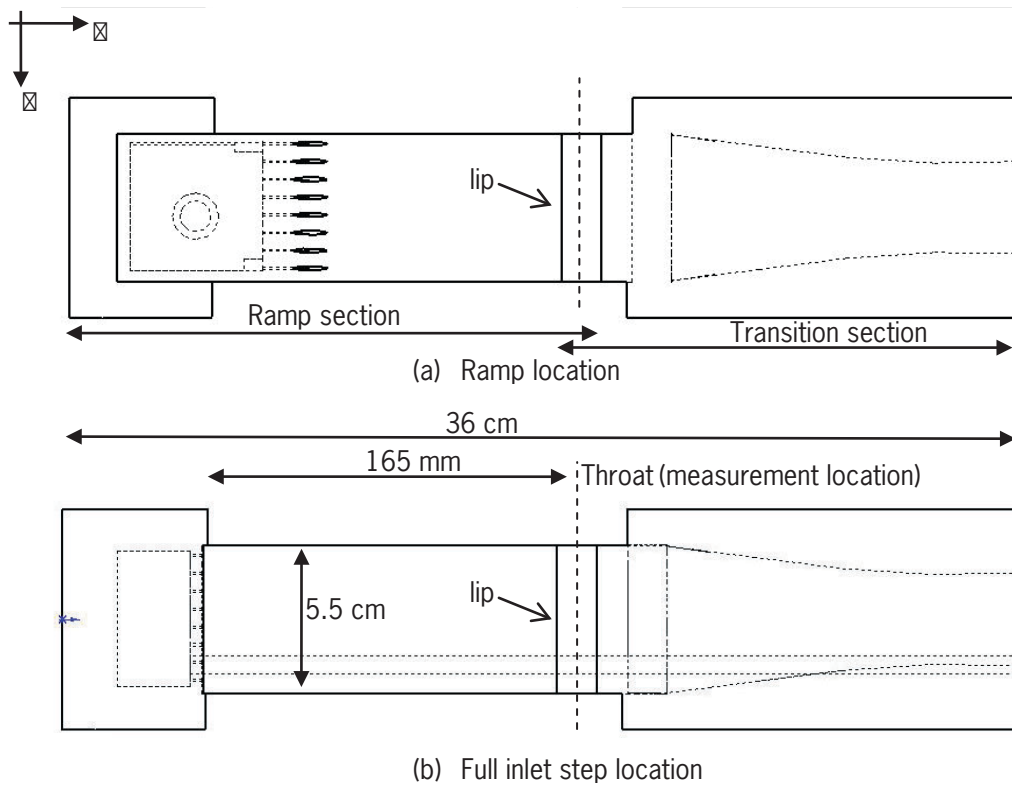


Figure 3: Top view (from the positive y axis) of the hole location and the overall configuration of the inlet system.

2.1. Laser Doppler Velocimetry

The backward scattering laser Doppler velocimetry (LDV) system allowed all three velocity components to be resolved within the submerged inlet. A Dantec® FiberFlow Probe, with a 112 mm diameter head and 5-beams, was used to measure the three velocity components. A 5 Watt Argon-ion laser provided the light source for the LDV. The Dantec® FlowMap software was used to process the raw data that was exported for the visualization, through the conversion matrix given in Equation 1. A traverse (Dantec® lightweight traverse) was used to position the laser within the inlet and control the grid locations at which data points were obtained. The traverse allowed a grid, precise to ± 0.05 mm, to be made in the specified planes of interest.

The power of each of the beams was maximized and balanced. Beam wavelengths of 476.5(violet), 488(blue), and 514.5(green) nm were employed for the velocity measurements corresponding to the measurements of u_2 , u_1 and u_3 respectively. The beam pattern (5-beams) was a cross with the center consisting of an overlapping green and blue beam. The two violet beams were aligned parallel to the y -axis. The green and blue beams were nearly coplanar in the x - z plane, with the green in the downstream position and the blue in the upstream location. The specific angles of the beam intersection were set by the 310 mm lens.

The beam spacing was nominally 37 mm for the 514.5 nm and 488 nm beams and 74 mm for the 476.6 nm beam [19]. The green and blue beam had a half angle of 3.40° and the violet an angle of 6.78° [20]. This provided the probe volumes given in Table 2. During the beam alignment, it was noticed that the blue and green beams were not collinear. The small out-of-plane angle was measured using the projection on the screen. The w -component was corrected for this bias in the transformation, given in Equation 1.

$$\begin{Bmatrix} u \\ v \\ w \end{Bmatrix} = \begin{bmatrix} -0.5009 & 0 & -0.5009 \\ 0 & 1.0 & 0 \\ 8.425 & 0.10 & 8.0425 \end{bmatrix} \begin{Bmatrix} u_1 \\ v_2 \\ w_3 \end{Bmatrix} \quad (1)$$

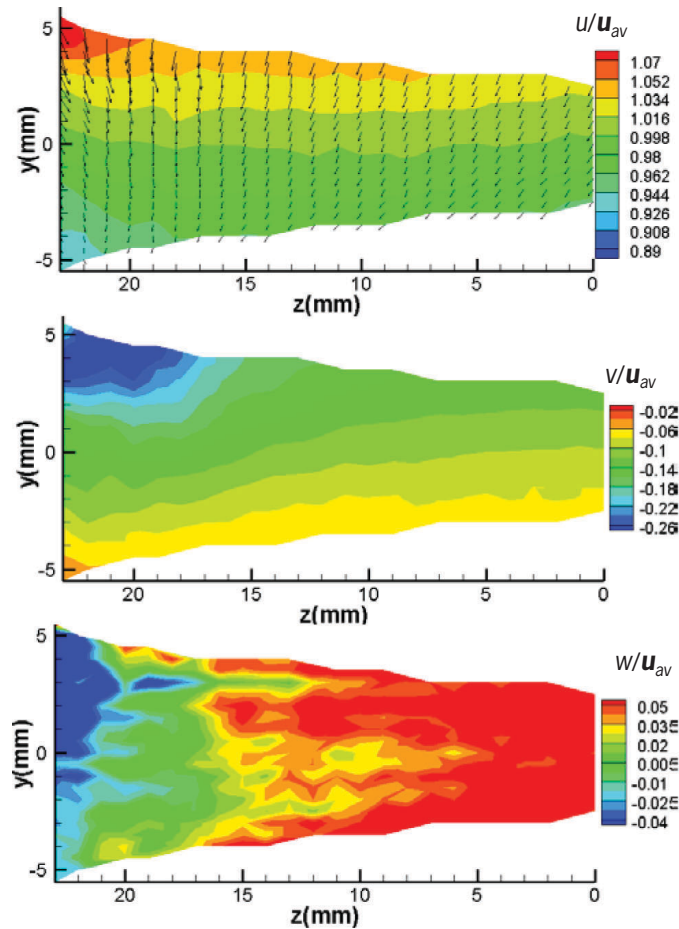
Table 2: The dimensions of the probe volume for the FiberFlow LDV probe.

	Violet	Blue	green
dx (mm)	0.046	0.047	0.050
dy (mm)	0.046	0.047	0.050
dz (mm)	0.388	0.792	0.835

The transformation matrix was altered by substituting 0.1 for 0 in the second column of the third row. This is equivalent to a correction for an approximately eight degree offset, which was consistent with the observed beam displacement. The magnitude of the w -component was the least accurate of the three components, due to the small angle made with the flow (3.402°); it is sufficient to illustrate the general trend and provide proof of the streamwise vortices [21]. The small angle has minor effects in the calculation of the u -component but significant effects in the w -component, derived from $1/(2 \sin 2\phi)$ [20]. The power and photomultiplier were set to maximize the particle count and rate for the LDV without vaporization of the particles.

2.2. Liquid Nitrogen Steam Seed Particles

The seeding was important for this experiment, due to the LDV system's requirements. The particles needed to follow the flow accurately and not impede the data rate by being too dense or collecting on the sidewalls, restricting the beam's access. Innovative Scientific Solutions Incorporated (ISSI) proposed the concept of a clean seeding that met both criteria for this situation [22]. The seeding was formed by steam particles that were rapidly condensed by liquid nitrogen. Proof of concept for the seeding technique is given in Reeder et al. [22]

Figure 4: Mean velocity components for the straight step configuration without flow control. ($u_{av}/u_\infty = 3.5$)

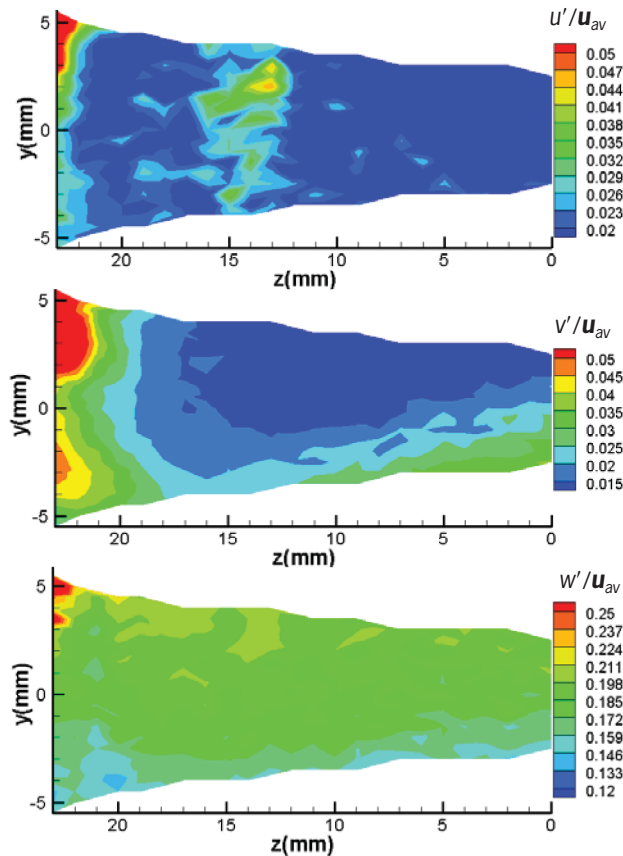


Figure 5: RMS velocity components for the straight step configuration without flow control. ($u_{av}/u_{\infty}=3.5$)

3. RESULTS

3.1. Straight Step Zero Mass Addition

The zero mass addition straight step configuration was the baseline study for the flow control examination. The discrete holes were examined to ensure that the jets were mixing to cover the entire width (z -direction) of the ramp. The mean velocity profile for the inlet with the flow control at 0% is shown in Figure 4. The measurement regions are trapezoidal rather than rectangular due to beam blockage. The u -component and the v -component have a gradient in the velocity in the y -direction. The streamwise u -component has higher velocities near the lip of the inlet while more sluggish flow is near the ramp where the boundary layer affects the flow. A region of particularly low velocity, $u = 0.94u_{av}$, is shown in the u -component in the ramp-sidewall juncture, $(y,z) = (0-5,23)$. The secondary flow has been superimposed on the u -component to indicate how the secondary flow affects the streamwise velocity profile and hence the pressure uniformity of the compressor face [23]. Here, the term “secondary flow” refers to the v and w components of the flow in a given y - z plane (i.e., normal to the x -direction). The v -component, shown in the middle of Figure 4, has a larger downward velocity near the lip side ($y = 5$ mm) that gradually decreases as it approaches the ramp. The downward velocity is due to the measurement region being slightly forward of the throat so the ramp imparts a downward direction. The w -component, shown in the bottom of Figure 4, has a gradient in the z -direction, with negative flow near the sidewall ($z = 23$ mm) and flow towards the wall near the center ($z = 0$). The w -component is twice the measured v -component velocity, demonstrating the accuracy limitation for this measurement. The w -component will be examined for general flow behavior. The vector plot does not show the expected circulation region from the near wall vortex predicted in Taylor [11]. Only a downward flow along the wall is evidenced, which is supported by measurements of the v and w -components. It is believed the vortex was never formed due to the high relative inlet velocity compared to the free stream velocity. The ratio is normally closer to one, whereas the inlet to free stream velocity of 3.5 in this experiment is closer to takeoff and landing conditions. The vortex never formed since the flow over the sidewall was simply drawn into the inlet.

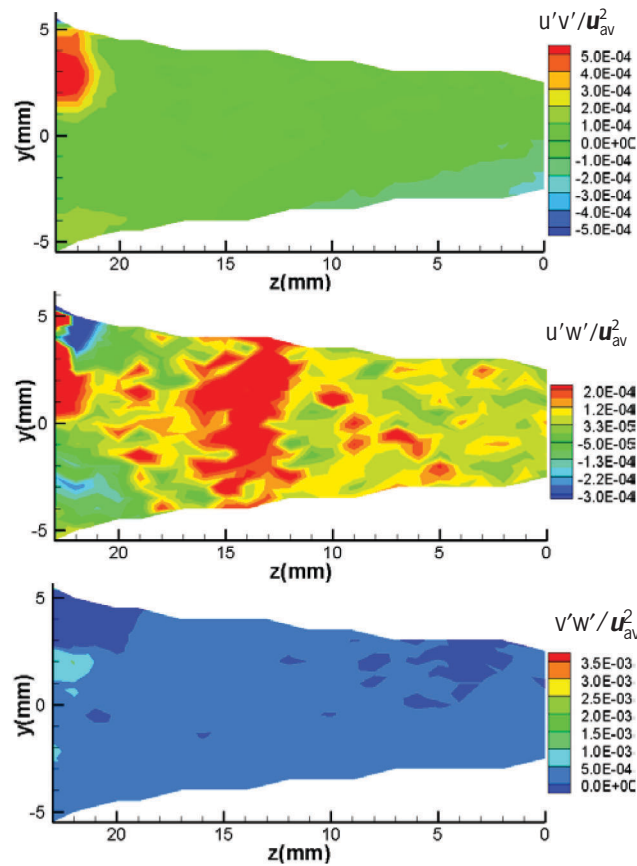


Figure 6: Reynolds shear stresses for the straight step configuration without flow control. ($u_{av}/u_{\infty}=3.5$)

The fluctuating velocity components for the straight step configuration are given in Figure 5 for the \bar{u}' , \bar{v}' , and \bar{w}' -components. The \bar{u}' -component is uniform with values of $0.02u_{av}^2$ over the entire measurement region. The higher fluctuations of $u' = 0.05u_{av}$, are relegated to the wall region where the downward flow occurs over the sidewall of the submerged inlet. The \bar{v}' -component has a similar range of values for the magnitude of the velocity fluctuations varying from $0.015-0.05u_{av}$, showing that the flow is isotropic, since the values are small and similar in range. The \bar{v}' -component has more variation occurring within the flow field where the ramp and sidewall interact. The highest fluctuations are near the sidewall where the downward flow interacts with the main inlet flow and the ramp. The main or core flow region where the boundary layer does not interact with the inlet flow has low fluctuations in comparison, with values near the free stream turbulence intensity [22]. The \bar{w}' -component is an order of magnitude higher than the \bar{u}' and \bar{v}' -components, five times the maximum measured value. The \bar{w}' -component has lower fluctuations along the ramp with higher fluctuations towards the lip side of the inlet. Consistent with the \bar{u}' and \bar{v}' -components, the fluctuations are higher near the wall on the lip side of the inlet. The addition of the \bar{v}' -component lends information that is normally not obtained in measurements where only the free stream velocity is obtained. The w -component is helpful if taken with regard to general flow trends. The energy distribution is revealed by the combination of the three components, which is something that is generally not achieved in experimental studies.

The remaining information on the energy content for the submerged inlet profile is revealed in the Reynolds shear stress components of $\overline{u'v'}$, $\overline{u'w'}$, and $\overline{v'w'}$. The shear stress stresses for the zero mass addition straight step configuration is given in Figure 6. The $\overline{u'v'}$ component, at the top of Figure 6, has low energy for the majority of the inlet interior. The only exceptions occur at the sidewall where the downward moving fluid affects the core and along the ramp with the growing boundary layer creating a velocity deficit. The maximum energy seen is $\overline{u'v'} = 5 \cdot 10^{-4} u_{av}^2$ at the sidewall and the minimum was $-2.5 \cdot 10^{-4} u_{av}^2$. The $\overline{u'w'}$ -component has little information that can be discerned. The difficulty with the $\overline{w'}$ -component obscures any relevant details about the flow field. The only thing that can be determined is that the higher magnitude energy entering over the sidewall is present. The $\overline{v'w'}$ -component is less

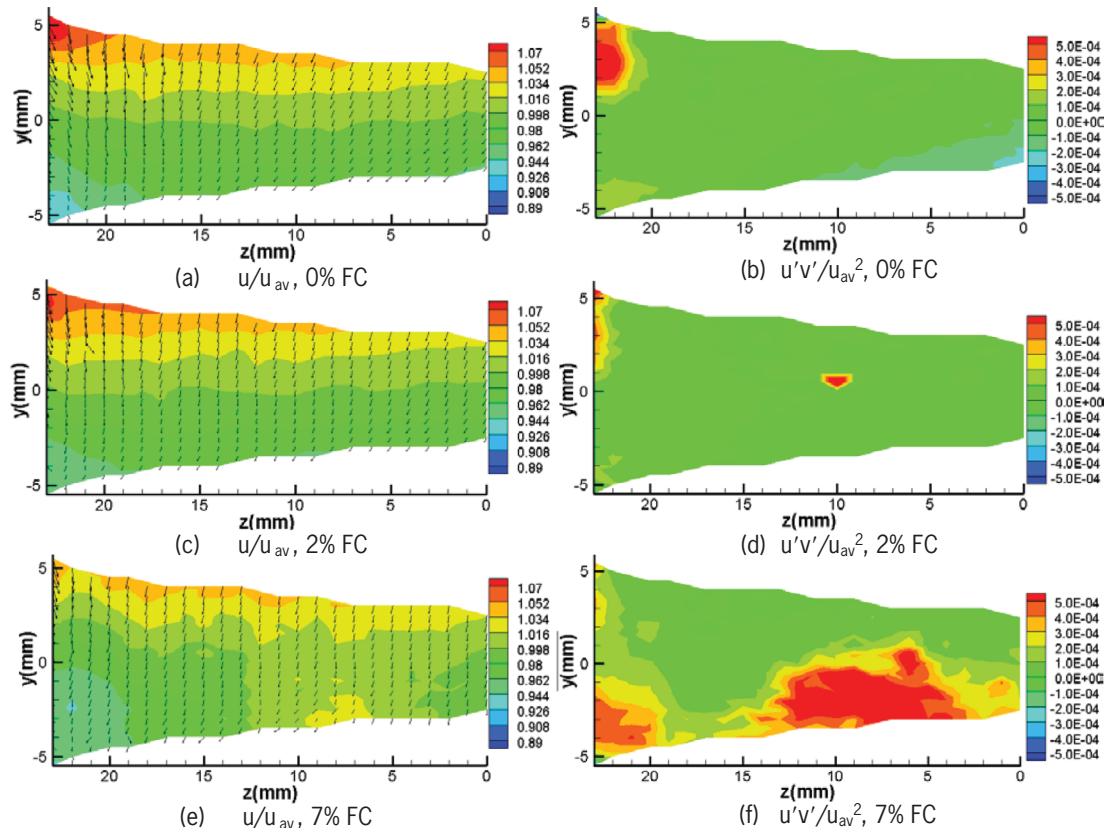


Figure 7: Mean velocity component and $\overline{u'v'}$ -component of the Reynolds stress with flow control (FC) addition for the straight step configuration. ($u_{av}/u_{\infty}=3.57$)

informative due to the correlation of two low velocities. The difficulty in obtaining the measurement appears in the order of magnitude higher scale of the $v'w'$ -component. The energy appears to be relatively uniform with only the flow over the sidewall being evident in the region where $(y,z)=(-3,23)$.

The $\overline{uw'}$ and the $\overline{vw'}$ are of less value than the $\overline{uv'}$ due to the mentioned limitations in obtaining the w -component of the velocities. These components were shown for completeness, but for the rest of the paper will not be given since they do not lend much insight into flow control configuration effectiveness. The u , v , $\overline{u'}$, $\overline{v'}$ and $\overline{u'v'}$ components were sufficient to evaluate the performance of mass flow addition. In particular the u -component and the $\overline{u'v'}$ component display the effect of the flow control while demonstrating the effects in all components of interest. The u -component is shown to display the small changes that occur due to the mass flow addition with respect to flow uniformity. The v -component also changed in a relatively minor manner. The energy content is the most visually demonstrative of the effect of the flow control, which was due to the fact that the energy requires more time to dissipate than the momentum. The $\overline{u'v'}$ -component was used to demonstrate the effect of the flow control addition for both the $\overline{u'}$ and $\overline{v'}$ -components. The flow profile of the components not shown have similar behaviors to the baseline profiles shown. Less velocity variation for the v and w -component was observed for the mass flow addition. For the $\overline{u'}$ and $\overline{v'}$ -components there was greater energy along the sidewall and ramp with the energy starting to overtake the free stream turbulence intensity near the lip.

3.2. Straight Step Mass Flow Addition

The effect of the flow control on the straight step configuration is evaluated based upon the u and $\overline{u'v'}$ -components in Figure 7. Mass flow additions, m_r , below 2% were found to be ineffective in preliminary studies so no measurements were obtained. For the step configurations $m_r = 5\%$ was found to be no different than the 2% addition. The addition of flow control to the inlet decreases the gradient of the streamwise, u -component. The range decreases from $u=0.89$ to $1.07u_{av}$ in Figure 7(a) to a range of 0.962 to $1.052u_{av}$ in Figure 7(c), with 2% addition. The range decreases further to 0.926 to $1.034u_{av}$ in Figure 7(e) with 7% mass flow addition. The result of the straight step configuration is an increase

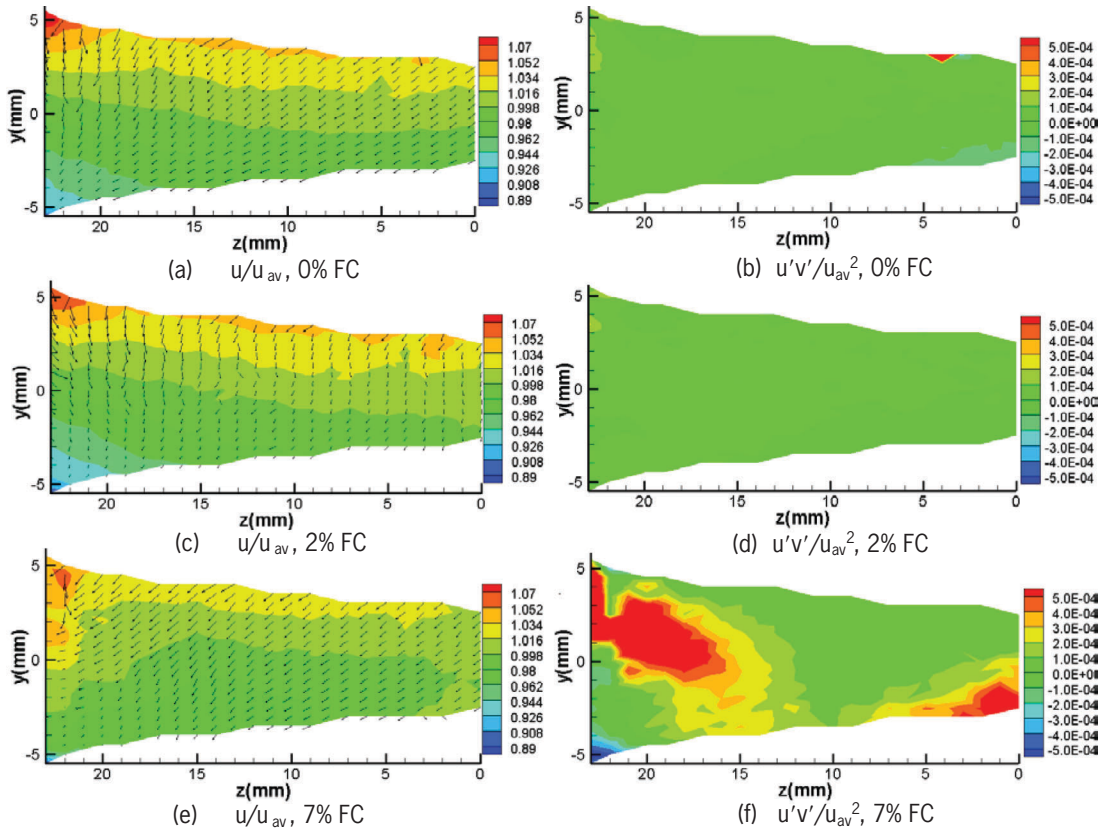


Figure 8: Mean streamwise components with the addition of flow control for the fanned step configuration and $\overline{u'v'}$ Reynolds shear stress. ($u_{av}/u_{\infty}=3.70$)

in area of the low velocity region at the ramp-sidewall juncture. The flow control has a visible effect on the inlet in altering the velocity gradient and appeared to induce a higher region of velocity along the ramp at $z = 7$ mm; demonstrating that the boundary layer deficit along the ramp has been overcome by the flow control. The secondary flow, as represented by the vectors in the u -component profiles for the v and w -components, are predominantly downward without any other visible movement. Stray vectors are artifacts of the difficulty in obtaining the w -component and beam distortion.

The flow control altered the energy content at the sidewall region and along the ramp. The low $\overline{u'v'}$ -component along the ramp is consistent with the boundary layer region, verifying measurement accuracy which was shown in the 0% addition case in Figure 7(b). The region near the sidewall has a pronounced decrease in the area of the maximum with a reduction in peak magnitude from $5 \cdot 10^{-4}$ to $4 \cdot 10^{-4} u_{av}^2$ in Figure 7(d). The mass flow addition increased the energy along the ramp so that the magnitude around $10^{-4} u_{av}^2$. The $m_r = 7\%$ has the most dramatic result, since the boundary layer deficit has been overcome as shown in Figure 7(f). The energy along the boundary layer has become positive and affected the flow field to the centerline ($y = 0$) location. The maximum region of energy corresponds to the location of increase in the u -component of Figure 7(e). The trends of increasing uniformity of the u -component and shear stress following with increasing mass flow addition are expected for the other flow control configurations.

3.3. Fanned Step Mass Addition

The fanned step configuration with the addition of flow control is shown in Figure 8 for the u and $\overline{u'v'}$ -components. The gradient in the y -direction and range of the u -component for the zero addition case, as shown in Figure 8(a), is similar to that seen for the straight step configuration in Figure 7(a). The model change of the ramp section did not alter the flow profile. The slower velocity is evident at the ramp-sidewall in Figure 8(a), with the secondary flow being predominantly downward. The w -component presented some difficulty but the relative movement can be neglected due to the measurement complications. The addition of flow control in Figure 8(c) reduced the range of the u -component, with

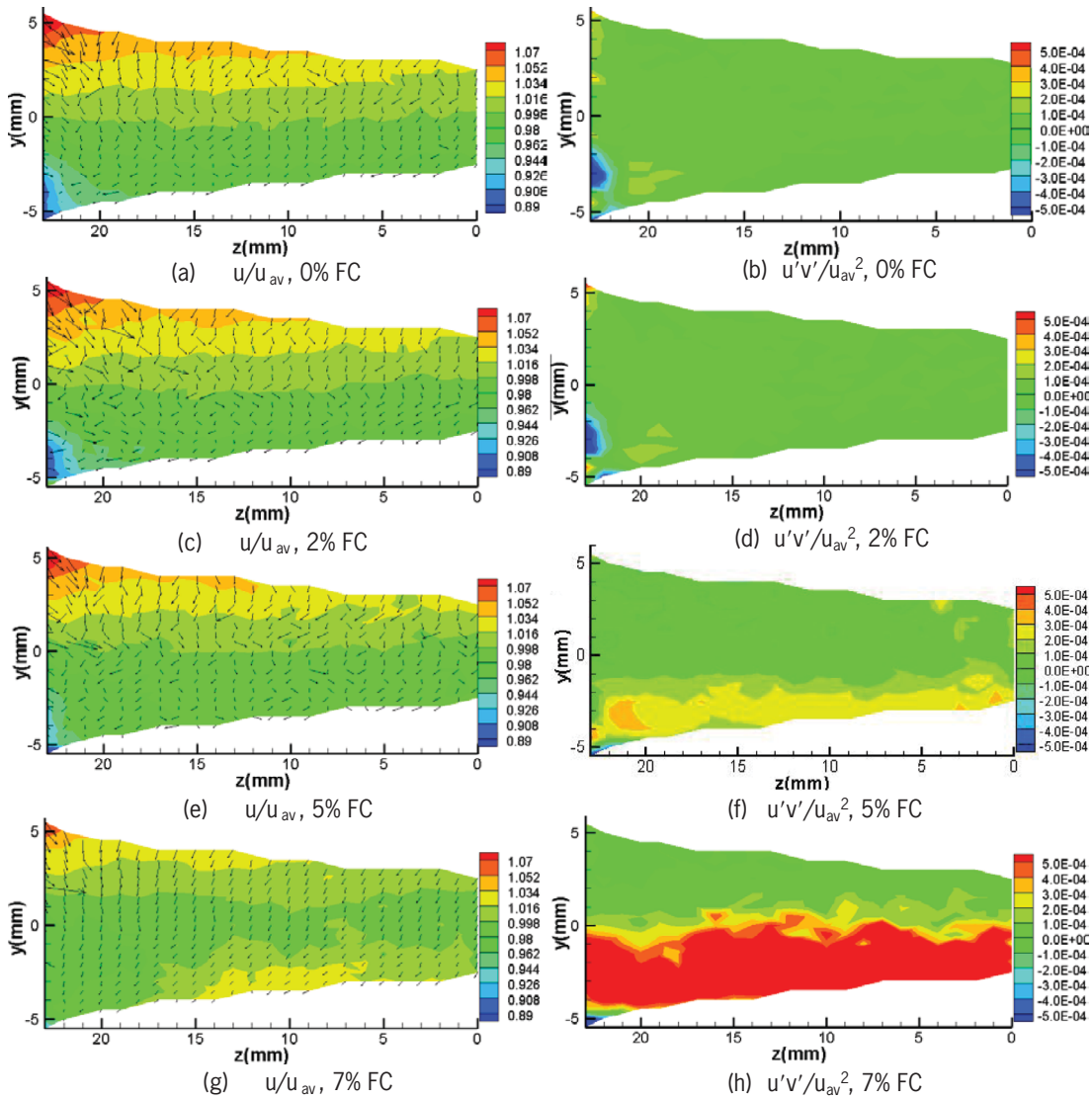


Figure 9: Mean streamwise component and $\overline{u'v'}$ Reynolds stress with flow control addition for the straight ramp configuration. ($u_{av}/u_{\infty}=3.76$)

the maximum dropping from 1.07 to $1.052u_{av}$. The $m_r = 7\%$ is more pronounced with less of the $1.052u_{av}$ region present with the minimum increasing from 0.926 to $0.944u_{av}$ in Figure 8(e). The high velocity region along the sidewall migrated towards the centerline ($y = 0$) with the mass flow addition. The flow control performed as hoped by increasing the inlet uniformity. This is denoted by having a smaller range in velocity variation.

The energy content is relatively uniform without flow control being near the free stream levels, as observed in Figure 8(b). The downward moving flow along the wall is smaller than that of the straight step configuration. The low energy content along the ramp is still in evidence with the same magnitude of $\overline{u'v'} = -3 \cdot 10^{-4}u_{av}^2$. The $m_r = 2\%$ changes little in the energy profile, other than a slight increase along the ramp, raising the value to $10^{-4}u_{av}^2$, as shown in Figure 8(d). The effect of the flow control is most prominent at the 7% addition, where the energy has become positive, as observed in Figure 8(f). The angled nature of the jets directed more momentum toward the wall and lifted the energy away from the ramp surface near the sidewall. The energy from the jets being near the wall and in the $+y$ region of the inlet, accounts for the increased velocity extending downward along the sidewall in Figure 8(e). The pronounced direction of the secondary flow towards the sidewall, particularly in the near wall region ($z = 18-23$ mm) where measurements are easier to obtain, is produced by the directionality of the introduced flow control.

3.4. Straight Ramp Mass Addition

The ramp configurations were expected to have more effect at the throat since they were positioned closer, so the 5% m_r cases were examined and are provided for the straight ramp configuration in Figure 9. The effect of the flow control on the streamwise component, u , are shown in Figure 9(a), (c), (e) and (g) for the 0, 2, 5 and 7% mass flow additions. The 2% m_r case, shown in Figure 9(c), does not evidence any change from the zero addition case since the magnitudes are fairly similar. The immediate shearing of the jets by the incoming flow may have mixed the added momentum of the flow control jets more rapidly than that of the step, preventing the mass addition from having an effect at the throat. Figure 9(e) with 5% addition increased the velocity along the ramp to be that of the medium velocity flow region of $0.98u_{av}$, aside from the ramp-sidewall juncture. The 7% m_r has a pronounced higher velocity region along the ramp that is centered at $z = 10$ mm and is near the maximum magnitude at a value of $1.034u_{av}$, as shown in Figure 9(g). This region of high velocity is an indication that too much flow control was used, since the flow is becoming less uniform. The secondary flow vectors are more random in these measurements since there was no significant flow organization. The flow has a downward trend and is of the same relative strength as the other configurations. The removal of the step did not drastically alter the mean velocity profile since the zero addition case has the same behavior as that observed for the step configurations.

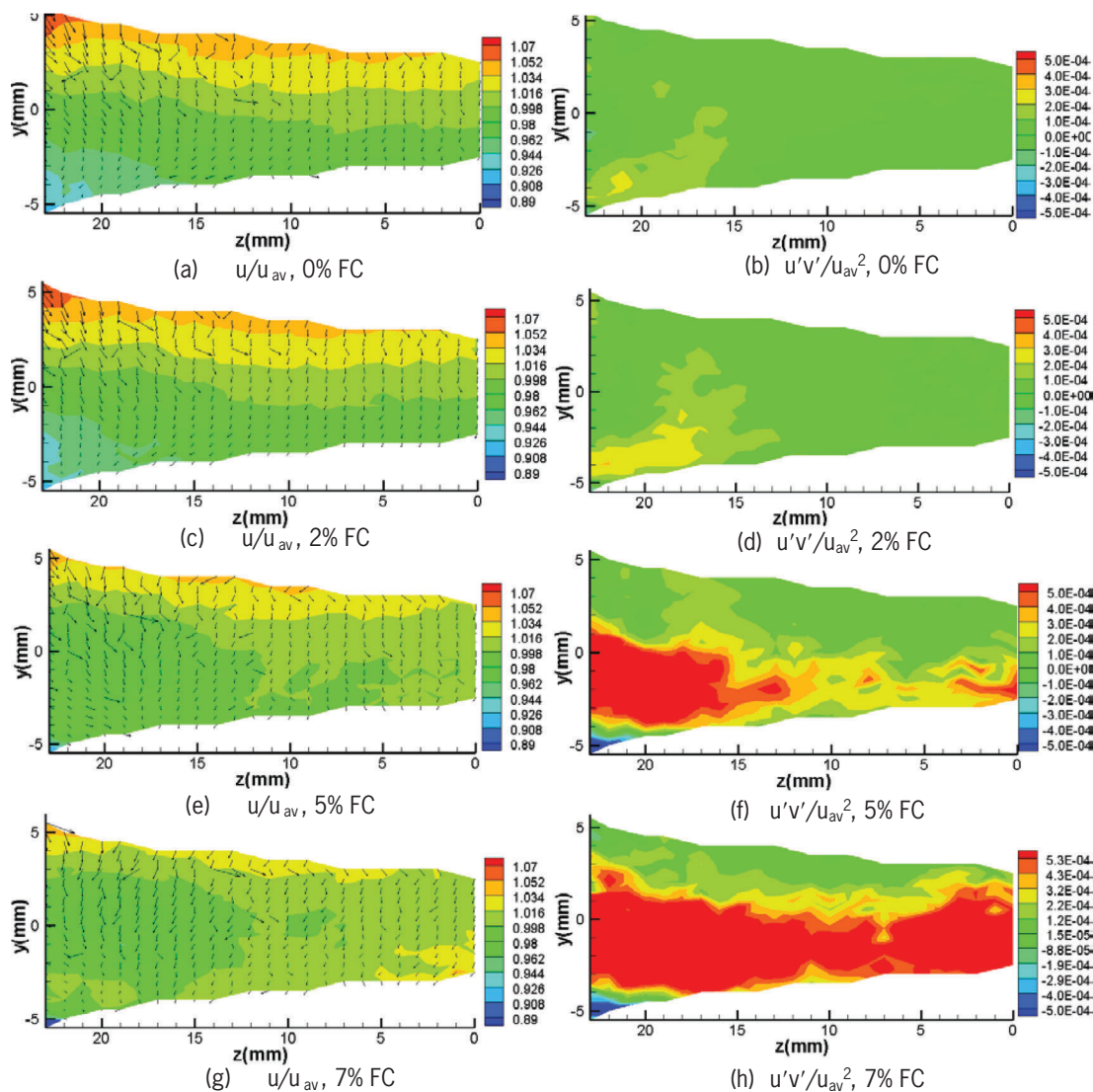


Figure 10: Mean streamwise component and $\overline{u'v'}$ Reynolds stress with flow addition for the fanned ramp configuration. ($u_{av}/u_{\infty}=3.64$)

The energy for the straight ramp configuration is shown in Figure 9(b), (d), (f), and (h). The $\overline{u'v'}$ energy is fairly uniform and near zero over the entire measurement of the zero addition case, with only a small negative region near the ramp-sidewall, as shown in Figure 9(b). The 2% m_r , shown in Figure 9(d) is essentially unchanged, supporting the theory that the energy was rapidly dissipated from the cross-flow the jets encountered upon exiting, since the jets did not have the strength to persist to the measurement region. The turbulent energy was measureable at 5% mass flow addition, as shown in Figure 9(f), and has a nearly uniform positive energy content along the ramp. The addition of 7%, given in Figure 9(h), increases the energy uniformly over the ramp to $5 \cdot 10^{-4} u_{av}^2$. The interesting thing to note is that the energy remains in the lower half of the inlet for the straight ramp configuration. This was not the case for the angled step configuration, since the turbulent energy crossed the y -centerline. It will be interesting to observe if this holds true for the angled ramp configuration. The energy was uniformly distributed along the measured ramp region, not consisting of localized pockets of higher energy as found in the step configurations. This suggests that the cross-flow aided in mixing the jets, despite the step configuration having more time to develop. The angled ramp configuration will aid in proving or disputing this supposition.

3.5. Fanned Ramp Mass Addition

The fanned ramp configuration for the u and $\overline{u'v'}$ -components with mass flow addition are given in Figure 10. The zero mass addition fanned ramp configuration is largely what was expected from the step and ramp configurations. The flow is predominantly downwards for the secondary flow vectors, with the streamwise component having a velocity gradient in the y -direction. The downward flow at the sidewall is also greater than the general flow in the rest of the submerged inlet profile. The 2% and the zero addition streamwise components, u , are essentially the same, as shown in Figure 10(c) and (a) respectively. The maxima and minima are of the same magnitude and the range has not been affected by the 2% addition. The effect of the flow control is demonstrated in the 5% m_r case, given in Figure 10(e). The low velocity region along the ramp and in the ramp-sidewall juncture is completely eliminated. The region near the center ($z = 0$) evidences an increased velocity that is greater than the inlet's average velocity. The 7% mass flow addition has the maximum measured velocity of $1.034 u_{av}$ along the ramp, which indicates that an over addition of momentum is probable.

The energy content in the $\overline{u'v'}$ shear stress supports this theory. The zero addition case in Figure 10(b) is fairly unremarkable, with few defining features. One feature is missing in the energy content; the downward moving flow along the wall did not induce a higher or lower energy region at the sidewall as occurred in the other configurations. Rather there is a slight positive region near the ramp corner as

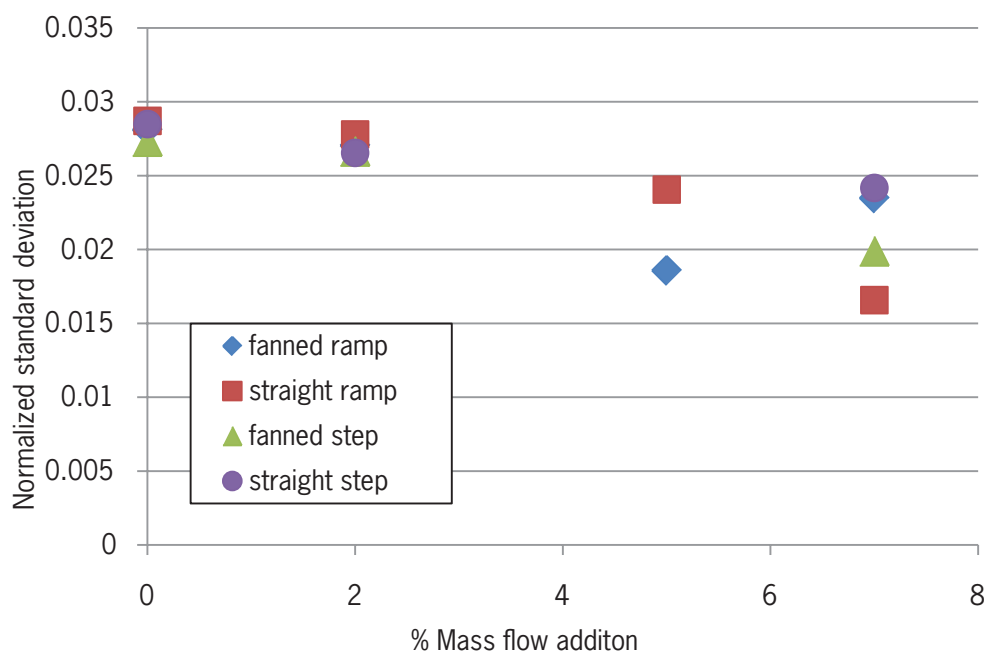


Figure 11: Dimensionless spatial standard deviation of the streamwise velocity for each flow control design with increasing mass flow addition.

shown in Figure 10(b). The angled configuration has more persistence than the straight configuration; some evidence of the 2% flow control is visible in Figure 10(d). The energy is positive along the entire z -direction in Figure 10(f) for an addition of 5%, however, it is lower than the maximum in the region from $z = 4$ to 10 mm. The higher energy near the wall crosses the y -centerline as occurred with the angled step configuration. The angled configuration is affecting the ramp-sidewall juncture as was desired to eliminate the lower velocity in this region. The 7% m_p , shown in Figure 10(h), has a uniformly high energy content along the ramp of the submerged inlet. The energy traverses over the y -centerline ($y = 0$) and affects the upper half of the inlet, particularly at the sidewall. The higher turbulence levels support the mixing that occurred in the u -component and the higher velocities found along the ramp.

3.6. Analysis of Flow Control Geometries

In all configurations the flow control was observed to affect the boundary layer in the submerged inlet. The figures are not clear which configuration was optimum. The step configurations appeared to require seven percent mass flow addition, while the ramp configurations required approximately 5% to obtain the most uniform u -component velocity profile. In order to quantify the effects of the flow control, the spatial variation or spatial standard deviation of the measurements were taken for the inlet. The spatial variation calculation is given in Equation 2. The spatial variation examined the deviation of the dimensionless measurement component over all the measurement locations. The spatial deviation was performed for 360 measurement locations at the throat of the submerged inlet. The \bar{u} and \bar{v} -components were included in the spatial variation to observe their contribution to the $\overline{u'v'}$ -component. All flow control configurations are represented on one plot to facilitate comparison and determine the relative effects of the mass flow addition.

$$u_{sd} = \frac{1}{N} \sum_{i=1}^N \left(\frac{u_i}{u_{av}} - 1 \right)^2 \quad (2)$$

The spatial variation of the streamwise velocity, u , is given in Figure 11. The variation tends to decrease with the addition of flow control, which means that the velocity range is decreasing and becoming more uniform with the addition of flow control. The straight ramp configuration at 7% has the overall lowest variation of all of the flow control settings and configurations. The best configuration is the fanned ramp, however, since it uses the least amount of flow control to obtain a minimum variation in the

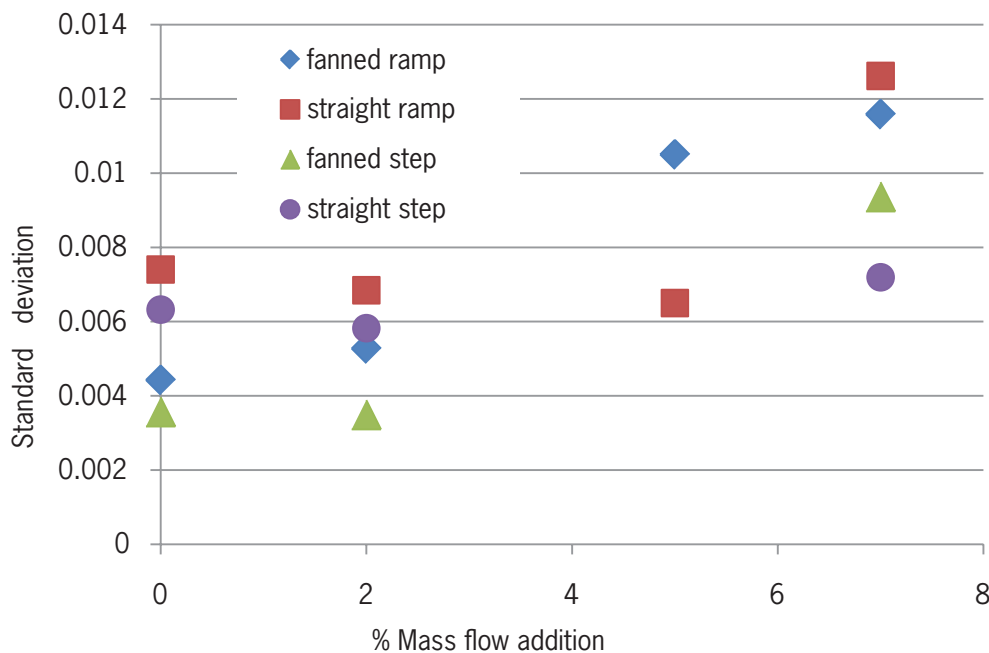


Figure 12: Spatial standard deviation of the dimensionless \bar{u}' component for each flow control design with increasing mass flow addition.

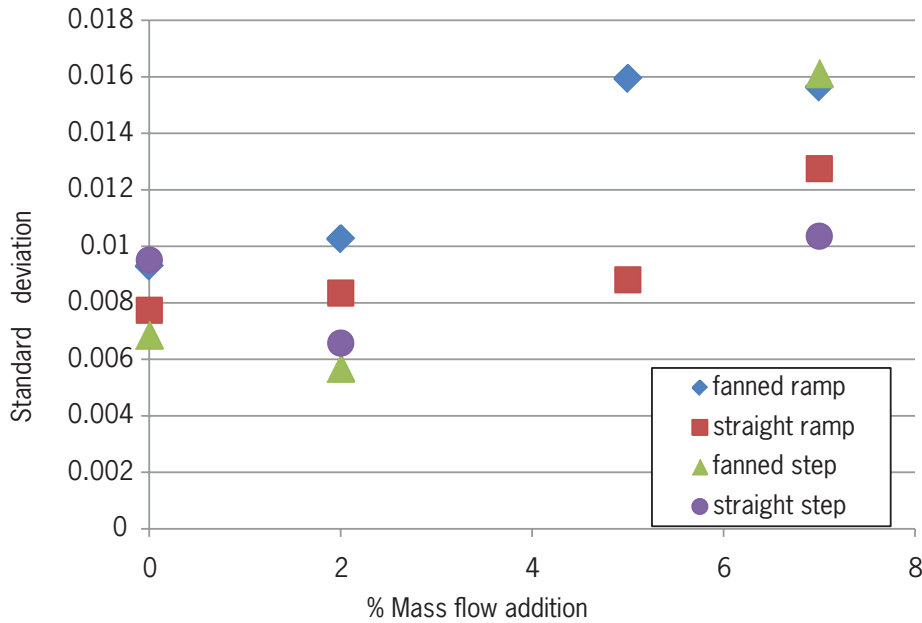


Figure 13: Standard deviation of the dimensionless \bar{v}' component and for each flow control design with increasing mass flow addition

streamwise velocity profile. The fanned ramp experiences a decrease in the uniformity with the addition of more flow control at 7%. This confirms that the 5% mass addition was the optimum for the fanned ramp geometry. The addition of too much mass flow addition can be detrimental. The best to worst performance for the flow control geometries is the fanned ramp at 5%, straight ramp at 7%, fanned step at 7% and then fanned ramp at 7% based on the streamwise uniformity given in Figure 11.

The spatial variation of the inlets for the u' -component displays increased fluctuations with the addition of m_p , as shown in Figure 12. The ramp configurations were, in general, higher than the step configurations as expected from proximity to the measurement region. The fanned ramp configuration was higher than the straight ramp configuration at the 5% case and slightly lower than the straight ramp configuration at the 7% mass flow addition. The \bar{v}' -component, shown in Figure 13, behaves similarly.

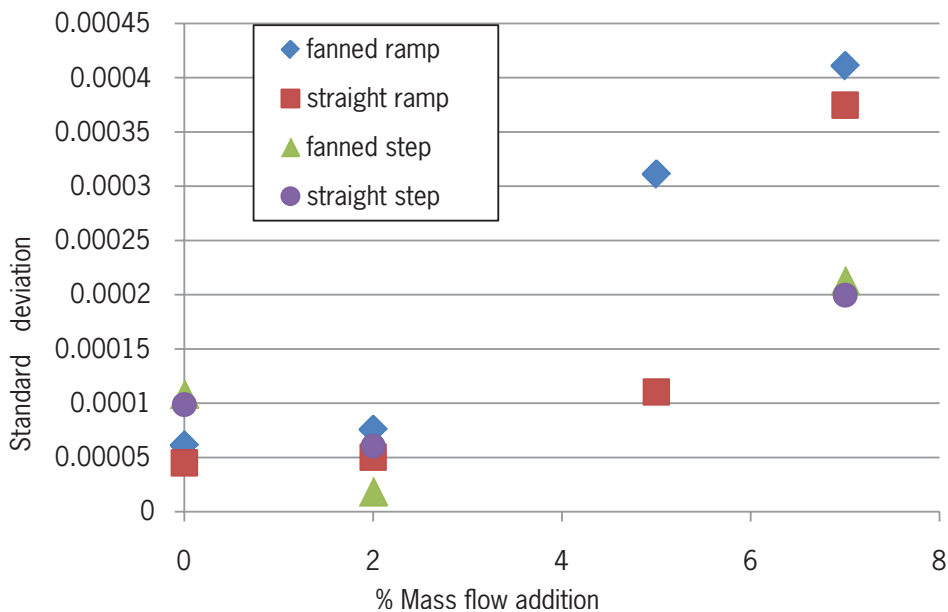


Figure 14: Standard deviation of the non-dimensionalized $\overline{u'v'}$ shear stress component for each flow control design with increasing mass flow addition.

The energy content increases with mass flow addition with the fanned configurations increasing more than the straight configurations. The straight step increased the least of the four ramp geometries, but does display an increase over the zero addition. Combining the effects of the $\overline{u'}$ and $\overline{v'}$ -components lead to a more pronounced increase in energy with the addition of flow control as shown for the $\overline{u'v'}$ -component in Figure 14. The same trends hold true from the $\overline{u'}$ and $\overline{v'}$ components. The fanned configurations have more energy than the straight configurations, and the ramp configurations contribute more than the step configurations. The energy does not help to identify which flow setting and configuration is the optimum since the energy will continue to increase with the mass addition as demonstrated in Figure 12 to 14. The spatial standard deviation of the streamwise velocity is the deciding flow variable to determine flow control performance, since the intent of the mass flow addition was to provide the most uniform velocity profile and hence the most uniform pressure face for the submerged inlet.

5. SUMMARY AND CONCLUSIONS

An examination of discrete flow control applied to a submerged inlet was carried out with the goal of improving flow uniformity at the inlet throat. Laser Doppler velocimetry studies of the inlet demonstrated that the velocity was low at the inlet floor for the baseline configuration. Active flow control, via blowing through discrete jets, led to improvements in that the velocity deficit measured at the inlet throat was reduced and, in some cases, eliminated. All three velocity components were measurable by the 5-beam LDV system, but the probe resolution in the spanwise (w -) component was limited and could only be used in a cursory manner.

Four different flow control geometries, each composed of eight discrete jets, were examined. For two configurations, the jets were fanned such that jets near the sidewalls were directed toward the sidewalls. The flow being directed at the sidewalls, as evidenced by the velocity profile near the sidewalls, led to a more uniform mean velocity distribution, better than their straight-jet counterparts. The influence of the flow control jets is also indicated by the higher turbulence levels shown in the $\overline{u'v'}/u_{av}^2$ as measured by the LDV system. In contrast to the mean velocity results, the effect of flow control was manifested by an increased level of turbulence. Thus, the $\overline{u'v'}$ turbulent component of the Reynolds stress was a clear indicator of the increased mixing within the boundary layer [24].

The spatial variation of the measured components proved to be insightful in assessing the effects of the flow control on the submerged inlet. The discrete jet configuration that performed the best was the fanned ramp configuration. For this case, the discrete jets were angled toward the sidewalls and the jets were positioned closer to the measurement region than the step configuration. For the conditions studied, the optimal uniformity was achieved with 5% mass addition for the fanned ramp case. An additional increase in mass flow for that configuration led to a velocity surplus near the floor of the inlet. Flow control applied along the ramp was found to be more effective than mass addition through jets positioned near the top of the ramp, presumably since the mass and momentum was added in closer proximity to the throat. In comparison to a previous study of a slot configuration at the same location, the discrete jets were comparable to the uniformity of the inlet profile for the same percent mass addition. To wit, the percentage of flow control necessary to eliminate the velocity deficit was 7.5% for the slot and 7% for the discrete jets [25].

Jet mixing theory worked well for predicting the flow uniformity of the jets and ensuring adequate coverage of the ramp was achieved over the length of the ramp to the throat of the submerged inlet. The location of the jets could potentially be moved closer to the throat so that a greater reduction in the mass flow ratio required to remove the velocity deficit is achieved.

ACKNOWLEDGMENTS

Thanks to all of the people who made this possible, particularly the laboratory support from Mr. Jay Anderson and Mr. John Hixenbaugh. Thanks as well to the Air Force Research Laboratory, Air Vehicles Directorate, Integration Branch for supporting this work and to our project monitor, Dr. Angela Scribber for providing helpful advice and assistance. This work was also supported through a Dayton Area Graduate Studies Institute fellowship.

REFERENCES

- [1] Martin, N. J. and Holzhauser, C. A., "An Experimental Investigation at Large Scale of Several Configurations of an NACA Submerged Air Intake," No. A8F21, National Advisory Committee for Aeronautics (NACA), Ames Aeronautical Laboratory, Moffett Field, California, October 1948.

- [2] Mossman, E. A. and Randall, L. M., "An Experimental Investigation of the Design Variables for a NACA Submerged Duct Entrances," No. A7130, National Advisory Committee for Aeronautics(NACA), Ames Aeronautical Laboratory, Moffett Field, California, January 1948.
- [3] Rolls, L. S., "A Flight Comparison of a Submerged Inlet and a Scoop Inlet at Transonic Speeds", No. A53A06, March 1953.
- [4] Rabe, A, Wing, N. and Burdisso, R., "Effectiveness of a Serpentine Inlet Duct Flow Control Technique at Design and Off-Design Simulated Flight Conditions," No. GT2004-53475, ASME Turbo Expo, Vienna Austria, June 2004.
- [5] Williams, T. and Cousins, P., "History, Philosophy, Physics, and Future Directions of Aircraft Propulsion System/Inlet Integration," No. GT2004-54210, ASME Turbo Expo, Vienna Austria, June 2004.
- [6] Sobester, A., "Tradeoffs in Jet Inlet Design: A Historical Perspective," *AIAA Journal of Aircraft*, Vol. 44, No. 3, May–June 2007, pp. 705–717.
- [7] Axelson, J. A. and Taylor, R. A., "Preliminary Investigation of the Transonic Characteristics of an NACA Submerged Inlet," No. A50C13, National Advisory Committee for Aeronautics(NACA), Ames Aeronautical Laboratory, Moffett Field, California, June 1950.
- [8] Divine, D.J., Watterson, J.K., Cooper, R.K., and Richardson, J., "An Investigation into Improving the Performance of Low Speed Auxiliary Air Inlets Using Vortex Generators," AIAA paper 2002-3264, St. Louis, Missouri, June 2002.
- [9] Lee, J.G., Jung, S.Y., Ahn, C.S., "Numerical Simulation of Three-Dimensional Flows for Flush Inlet," AIAA Paper 2004-5190, Providence, Rhode Island, August 2004.
- [10] Lee, B.J., Kim, C., Rho, O.-H., "Optimal Shape Design of the S-Shaped Subsonic Intake Using NURBS," AIAA paper 2005-0455, Reno, Nevada, January 2005.
- [11] Taylor, R.A., "Some Effects of the Side-Wall Modification on the Drag and Pressure Recovery of an NACA Submerged Inlet at Transonic Speeds", NACA, February 1952.
- [12] Jovanovic, V., Taskinoglu, E., Knight, D., Elliott, G., "Experimental Investigation of a Submerged Inlet," *AIAA Journal*, Vol. 22, No. 1, January 2006, pp. 214–217.
- [13] Jovanovic, V., Taskinoglu, E., Knight, D., Elliott, G., "Experimental Investigation of a Submerged Subsonic Inlet-Part II," No. 2004–4842, Providence, Rhode Island, August 2004.
- [14] Taskinoglu, E., Knight, D., "Design Optimization for Submerged Inlets- Part I," No. AIAA 2003–1247, Reno, Nevada, January 2003.
- [15] Florea, R., Hass, M., Lents, C.E., and Stucky, M.B., "Optimization of Bleed-Flow-Control for an Aggressive Serpentine Duct," , AIAA Paper 2005-1205, January 2005, 43rd AIAA Aerospace Sciences Meeting and Exhibit.
- [16] Vaccaro, J.C., Sanhi, O., Olles, J., Jansen, K.E., and Amitay, M., "Experimental and Numerical Investigation of Active Flow Control of Inlet Ducts," *International Journal of Flow Control*, Vol. 1, No. 2, pp. 133–154, 2009.
- [17] Wilson, D.G., Korankianitis, T., *The Design of High-Efficiency Turbomachinery and Gas Turbines, 2nd Edition*, Prentice Hall, 1998.
- [18] Glawe, D.D., Samimy, M., Nejad, A.S., and Chen, T.H., "Effects of Nozzle Geometry on Parallel Injection into a Supersonic Flow," *AIAA Journal of Propulsion and Power*, Vol. 12, No. 6, November-December 1996.
- [19] *Three-Color, Five-Beam, Three Component Laser Doppler Anemometer System*, Dantec Electronics, New Jersey, RFQ F33601-86-R-0297, August 1986.
- [20] Byrne, G.D., James, S.W., Tatam, R.P., "A Single-head Fibre Optic Laser Doppler Anemometer Probe for the Measurement of Flow Angles," *Measurement Sciences and Technology*, Institute of Physics Publishers, United Kingdom, No. 15, 2004.
- [21] Berger, S.A., Talbat, L., and Yao, L.-S., "Flow in Curved Pipes," *Fluid Mechanics*, 1983, pp. 461–512.
- [22] Reeder, M.F.; Crafton, J.W.; Estevadeordal, J.; DeLapp, J.; McNiel, C.; Peltier, D.; Reynolds, T., "Clean Seeding for Flow Visualization and Velocimetry Measurements." *Experiments in Fluids*, Vol. 48, No. 5, pp. 889–900, 2010.

- [23] *Gas Turbine Engine Inlet Flow Distortion Guidelines*, Aerospace Recommended Practices, Revision B, ARP (1420), SAE, Pennsylvania, 2002.
- [24] Wilcox, D. C., *Turbulence Modeling for CFD*, 2nd Edition, DCW Industries, California, 1998.
- [25] Scribber, A.R. and Goettke, M.K., *Reactive Conformal Inlet Technology Enhancement (RECITE)*, Integration and Demonstration Branch, Aeronautical Science Division, AFRL-RB-WP-TR-2008-3134, AFRL, July 2008.